Pergamon

Int. J. Heat Mass Transfer. Vol. 41, No. 14, pp. 2113–2124, 1998

Printed in Great Britain
0017–9310/98 $19.00+0.00

PII: S0017–9310(97)00354–2

On the evolution of double-diffusive intrusions into a stably stratified liquid: the physics of self-propagation

HENK A. DIJKSTRA† and E. JURJEN KRANENBORG

Institute for Marine and Atmospheric Research Utrecht, Utrecht University, The Netherlands

(*Received* 17 *March* 1997 *and in final form* 10 *November* 1997)

Abstract—This is the second part of a study of the nonlinear evolution of double-diffusive instabilities into laterally heated stably stratified liquids. Flows developing in initially doubly stratified systems are considered, i.e. in addition to a stabilizing salinity distribution a destabilizing temperature distribution is present. Although the development of the intrusions is qualitatively similar to that in singly stratified liquids, important differences occur when the initial destabilizing temperature gradient becomes large. When the lateral heating is turned off, intrusions are still able to propagate. The main contribution of the paper is a detailed study of the physics of this self-propagation process. © 1998 Elsevier Science Ltd. All rights reserved.

1. INTRODUCTION

Double-diffusive convection, i.e. convection in a stably stratified liquid due to different diffusivities of two components [1] is a potentially important mixing process of heat and salt in the ocean [2]. Clear signatures of this process are well mixed layers, separated by very stable interfaces over which only diffusive transport is possible. A typical case where these layers occur is a laterally heated liquid which is initially stably stratified through a constant vertical salt gradient. Laboratory experiments [3, 4] have provided the scales of these layers in terms of parameters of the flow. In the first part of this study, which was concerned with the layer merging process of intrusions developing in an initially singly stratified liquid [5], the experimental results were shortly reviewed. If the lateral temperature gradient is ΔT and the initial salinity gradient ϕ_0, then the characteristic layer scale is

$$\eta = \frac{\alpha \Delta T}{\beta \phi_0} \tag{1}$$

where α and β are the coefficients in the linear equation of state relating density changes due to temperature and salinity changes, respectively.

In experiments, also situations have been considered in which, apart from a stabilizing salt gradient $\phi_0 = -\partial S_0/\partial z$, a destabilizing temperature gradient $\partial T_0/\partial z$ was initially present [4, 6]. Motivation for these experiments was the potential ability to tap energy from the initial thermal stratification. Layers may continue to propagate even when sidewall forcing is turned off, a process called self-propagation. The doubly stratified systems are particularly interesting in an oceanographic context because the presence of an additional unstable temperature gradient is common in the upper parts of polar seas [7].

In ref. [4] the self-propagation of intrusions is anticipated for relatively low values of the stability ratio R_ρ, defined as

$$R_\rho = \frac{\beta \dfrac{\partial S_0}{\partial z}}{\alpha \dfrac{\partial T_0}{\partial z}}. \tag{2a}$$

However, even at the smallest value of $R_\rho = 2.5$, they did not observe it.

Extensive experimental and numerical work on the evolution of intrusions in doubly stratified systems was presented in ref. [6]. Instead of a wall temperature rise [4], ref. [6] uses a constant lateral heat flux forcing q. They classify the flows according to the values of R_ρ and a lateral stability parameter R_1, defined as

$$R_1 = \frac{\dfrac{\alpha q}{k}}{\alpha \dfrac{\partial T_0}{\partial z} - \beta \dfrac{\partial S_0}{\partial z}} \tag{2b}$$

where k is the thermal conductivity. In the case of high lateral and gravitational stability (small R_1 and large R_ρ, class I) the system behaves like the singly stratified case. Within the layers, the temperature is stably stratified and the salt is well mixed. As the lateral heating becomes more important (class II) con-

† Author to whom correspondence should be addressed. Institute for Marine and Atmospheric Research Utrecht, Utrecht University, Princetonplein 5, 3584 CC, Utrecht, The Netherlands.

NOMENCLATURE

A	aspect ratio
E_k	dimensionless kinetic energy
g	gravitational acceleration [m s^{-2}]
H	height of the container [m]
$\mathscr{H}_d$	dimensionless diffusive lateral heat transport
k	thermal conductivity [m^2 s^{-1}]
L	length of container [m]
Le	Lewis number
$\overline{Nu}$	vertically integrated Nusselt number
Pr	Prandtl number
R	buoyancy ratio
R_l	lateral stability parameter
R_ρ	vertical (gravitational) stability ratio
Ra_η	thermal Rayleigh number based on η
Ra_T	thermal Rayleigh number
S	dimensionless salinity
t	dimensionless time
t_0	dimensionless heat-up time
T	dimensionless temperature
U	dimensionless horizontal velocity
x	dimensionless horizontal coordinate
z	dimensionless vertical coordinate.

Greek symbols

α	thermal expansion coefficient [K^{-1}]
β	solutal expansion coefficient [-]
ΔS	vertical salinity difference [-]
ΔT	horizontal temperature difference [K]
η	internal vertical lengthscale [m]
κ_S	saline diffusivity [m^2 s^{-1}]
κ_T	thermal diffusivity [m^2 s^{-1}]
ν	kinematic viscosity [m^2 s^{-1}]
ρ	density [kg m^{-3}]
ϕ_0	initial salinity gradient [m^{-1}]
ψ	dimensionless streamfunction
ω	dimensionless vorticity.

Subscript

0	reference value.

vection becomes more vigorous and the layer thickness increases. The salinity is generally well mixed or slightly unstable stratified within the layers and convection due to salt-fingering is possible. In the case of very low gravitational and lateral stability (class III), both heat and salt are well-mixed within the layers. Under conditions of small R_ρ and relatively large R_l, self-propagation is observed.

In this paper, the evolution of intrusions into a doubly stratified liquid is studied through direct numerical simulation in a two-dimensional set-up. At a low stability ratio, self-propagation of intrusions is found and several characteristics of this process are obtained. Based on the analysis of the numerical results, two energy sources for the self-propagation are identified. First, local instabilities which develop ahead of the intrusions may provide energy used for the propagation. This source is similar to that proposed in ref. [6]. Another source of energy is shown to come from the global adjustment of the density field.

2. FORMULATION

The model is similar to that in ref. [5] but shortly repeated for convenience. A two-dimensional rectangular container (length L and height H) is filled with a Newtonian liquid with a kinematic viscosity ν and stratified through heat and salt with a constant thermal diffusivity κ_T and solutal diffusivity κ_S. The governing equations are non-dimensionalized using scales H, H^2/κ_T, κ_T/H, ΔS and ΔT for length, time, velocity, salinity and temperature, respectively. The equations describing the evolution of the flow are the two-dimensional Navier–Stokes equations and the conservation equations of heat and salt given in ref. [5] in terms of the streamfunction ψ and the vorticity ω.

Apart from the Prandtl number $Pr = (\nu/\kappa_T)$, the Lewis number $Le = (\kappa_T/\kappa_S)$ and the aspect ratio $A = (L/H)$, the relevant parameters in these equations are the thermal Rayleigh number Ra_T, the buoyancy ratio R, the length scale η and the Rayleigh number Ra_η based on η

$$Ra_T = \frac{g\alpha \Delta T H^3}{\nu \kappa_T} \qquad R = \frac{\beta \Delta S}{\alpha \Delta T}$$

$$\eta = H/R \qquad Ra_\eta = Ra_T/R^3. \tag{3}$$

At all boundaries no-slip conditions for velocity are prescribed. At the left sidewall, the heating curve is prescribed as

$$T(x = 0, z, t) = 1 - \exp\left(-\frac{t}{t_0}\right) \tag{4a}$$

and the right sidewall is assumed to be isolated. This situation is similar to that in the experiments by ref. [4]. All walls are impermeable to salt; in dimensionless form the remaining boundary conditions are

$$x = 0: \ \frac{\partial S}{\partial x} = 0 \qquad x = 1: \ \frac{\partial T}{\partial x} = 0, \ \frac{\partial S}{\partial x} = 0$$

$$z = 0: \ \frac{\partial S}{\partial z} = 0, \ \frac{\partial T}{\partial z} = 0 \qquad z = 1: \ \frac{\partial S}{\partial z} = 0, \ \frac{\partial T}{\partial z} = 0. \tag{4b}$$

Table 1. Values of both dimensionless and dimensional model parameters

Dimensionless quantities	
$A = 1$	$t_0 = 1 \cdot 10^{-3}$
$Le = 101$	$H = 0.2$ (m)
$Pr = 7$	$L = 0.2$ (m)
$R = 5$	$\kappa_S = 1 \cdot 10^{-9}$ (m^2 s^{-1})
$Ra_\eta = 5 \cdot 10^4$	$\kappa_T = 1 \cdot 10^{-7}$ (m^2 s^{-1})
$Ra_T = 6.25 \cdot 10^6$	$\nu = 7 \cdot 10^{-7}$ (m^2 s^{-1})

3. RESULTS

A 'reference' simulation is defined by the values of the parameters as given in Table 1. As in ref. [5], the thermal diffusion time scale is 4×10^5 [s] and all dimensionless times below are with respect to this time. The initial conditions are different from those in ref. [5] in that there is, in addition to a stabilizing salt gradient, now also a destabilizing temperature gradient. The initial conditions introduce the stability ratio R_ρ and become

$$t = 0: T_0(x, z) = -RR_\rho^{-1} z \quad S_0(x, z) = 1 - z. \tag{5}$$

The limiting singly stratified case is obtained as $R_\rho \to \infty$.

A value of $R_\rho = 1.5$ is potentially in the regime of self-propagation [6]. To be able to make comparisons with the singly stratified flows in ref. [5], the buoyancy ratio R is chosen such that the initial density gradient based on equation (5) is the same as the initial density gradient in the standard case in ref. [5] ($R = 5$); this results in $R = 15$. Due to the initial vertical temperature gradient, the lengthscale η and therefore the Rayleigh number Ra_η effectively vary linearly with z. The initial temperature distribution and Ra_η were prescribed such that at $z = 1/2$: $Ra_\eta = 5 \times 10^4$, which is the standard value in [5]. Hence, for $z < 0.5$ ($z > 0.5$) the buoyancy forcing is weaker (stronger) than that at $z = 0.5$, because the lateral temperature difference (between wall and liquid far from the heated wall) decreases with z.

3.1. *Flow characteristics*

We first consider a cavity with aspect ratio $A = 1$ as in ref. [5] and use the same numerical methods and the same resolution (201×201 equidistant grid-points). The layer development for the standard case $Ra_\eta = 5 \times 10^4$ and $R = 15$ is presented in Fig. 1, where four snapshots of the flow field are shown as contour plots of the streamfunction. More details of the flow can be observed in Fig. 2, where the difference of the actual salinity field and the initial salinity distribution are presented as a grey-shade plot. The latter salinity fields are also shown in Fig. 3 at corresponding times for the singly stratified case with $R_\rho = \infty$, $R = 5$.

In both singly and doubly stratified cases, layers develop within about 10 h. However, the initial development and the final scales of the layers are strikingly different for both cases. Whereas in the singly stratified case about six layers develop (Fig. 3(c)–(d)), the number of layers is smaller in the doubly stratified case. About four layers are observed (Fig. 2(c)–(d)), of which only the lower three are well-developed. For these three layers, the thickness increases upwards contrary to the layers in Fig. 3(c)–(d) whose thickness decreases upwards. The layer size is larger than that of the corresponding singly stratified flow, which is in accordance with the observations of ref. [4].

Plots of the horizontal velocity, temperature, salinity and density along a section through the middle of the container ($x = 0.5$) are shown at $t = 0.1$ for the doubly stratified case in Fig. 4. The horizontal velocities have a slightly smaller amplitude in the lower layer and nearly equal magnitude in the next two layers (Fig. 4(a)). Within each layer, the temperature is stably stratified whereas the salinity is well mixed (Fig. 4(b)). Over the interfaces separating the layers, the temperature is unstably stratified, similar to the distributions found in the singly stratified case [5]. The salinity profile in Fig. 4(b) also reveals the increase of layer thickness with height. The latter effect can easily be explained, since the layer thickness depends on the lateral temperature differencewhich varies with liquid height in the doubly stratified case. The density distribution is generally stable both in the layers and the interfaces between them (Fig. 4(c)).

The main difference between the flows in Figs. 2 and 3 is the convective activity in the upper layer which is much stronger for the doubly stratified case (compare Fig. 2(a)–(b) with Fig. 3(a)–(b)). Clear signatures of this strong convection are also shown in Fig. 1(b)–(c). These features were also noted by ref. [6] in their doubly stratified experiments. For instance, their Fig. 5(a) shows the same plume-like structures as those in Fig. 2. This strong convection is absent in the singly stratified case (Fig. 3). The existence of flow with significant convective activity suggests that the simulated flow would fit into either class II or III of ref. [6], and since the temperature is stably stratified within the layers (Fig. 4(b)), class II seems appropriate.

Although we prescribe no constant heat flux at the left wall, as in ref. [6], we determine the magnitude of the lateral stability parameter R_l by computing the range of the heat flux in the simulation. The parameter R_l, as given in equation (2b), can be expressed into our model parameters by nondimensionalization and using the values of the vertically averaged horizontal heat flux $\overline{Nu}(x, t)$ (defined in ref. [5]) at the heated sidewall ($x = 0$). This gives

$$R_l = \frac{\mathscr{H}_d \overline{Nu}(0, t)}{R(1 - R_\rho^{-1})} \tag{6}$$

where $\mathscr{H}_d$ is the diffusive heat flux in absence of any flow [5]. In the simulation above, with a temperature (4a) at the left sidewall, the heat transport varies sig-

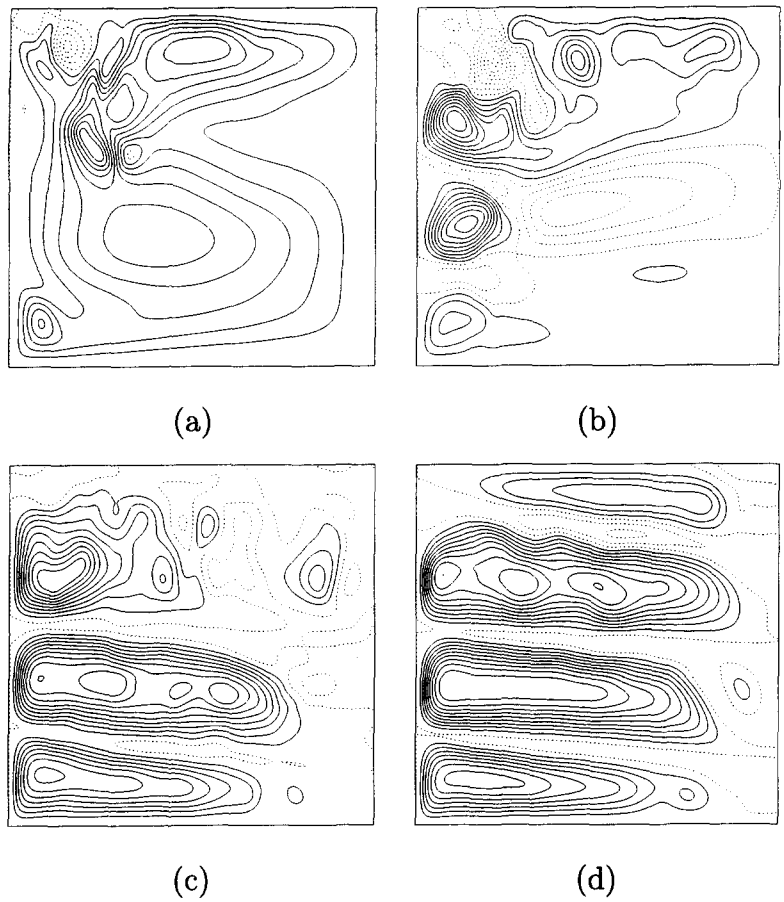

Fig. 1. Contour plots of the streamfunction, showing the development of layers in the doubly stratified case, $Ra_\eta = 5 \times 10^4$, $R = 5$; (a) $t = 0.005$; (b) $t = 0.01$; (c) $t = 0.05$; (d) $t = 0.1$.

nificantly along the heated wall because Ra_η effectively varies vertically. However, the value of R_l based on the averaged heat flux is in the range [4, 40]. For a typical case, with $\mathscr{H}_d Nu = 60$ ($t = 0.1$), $R = 15$ and $R_\rho = 1.5$, the stability parameter equals $R_l = 12$. Hence, a comparison with the experimental results in Table 2 of ref. [6] confirms that, considering the values of R_ρ and R_l, even for this large range of R_l the simulation falls into class II. For this regime, self-propagation is therefore possible, and we consider its existence in a slightly larger aspect ratio container.

3.2. *The analysis of self-propagation*

For the same values of the parameters as in the previous simulation, the evolution of the intrusions is investigated for a wide tank with $A = 4$. The numerical resolution in the simulations was chosen to be 401×101. This choice was determined by a desire to just resolve the salinity boundary layers but keep the computation manageable in terms of CPU time.

In these simulations, the thermal forcing at the left sidewall is maintained until $t = 0.05$. We present the flow development after $t = 0.05$ for three different cases in Fig. 5. In Fig. 5(a), the development of the flow has been plotted for the case that the thermal forcing is continued after $t = 0.05$. The layers continue to develop towards the right wall and the region of strong convective activity extends to nearly half the container. If for this case, the thermal forcing is stopped at $t = 0.05$, then still the layers continue to propagate towards the right (Fig. 5(b)). The latter is a clear signature of self-propagation and will be analysed below. For comparison, the evolution for the singly stratified case, for which the forcing is turned off at $t = 0.05$ is also shown (Fig. 5(c)). Self-propagation does not occur and the layers disappear due to viscous dissipation.

The flow in Fig. 5(b) is considered in more detail by vertical sections of the temperature, salinity and density at different horizontal positions within the layer. At $t = 0.05$, it is observed that heat and salt have been transported upwards within the upper layer in Fig. 5(b), such that the temperature distribution is stabilizing (Fig. 6(a)) and the salinity distribution (Fig. 6(b)) is slightly destabilizing. However, the liquid is still stably stratified (Fig. 6(c)) apart from some small intervals where it is unstably stratified. Hence, the main source of convective activity can be

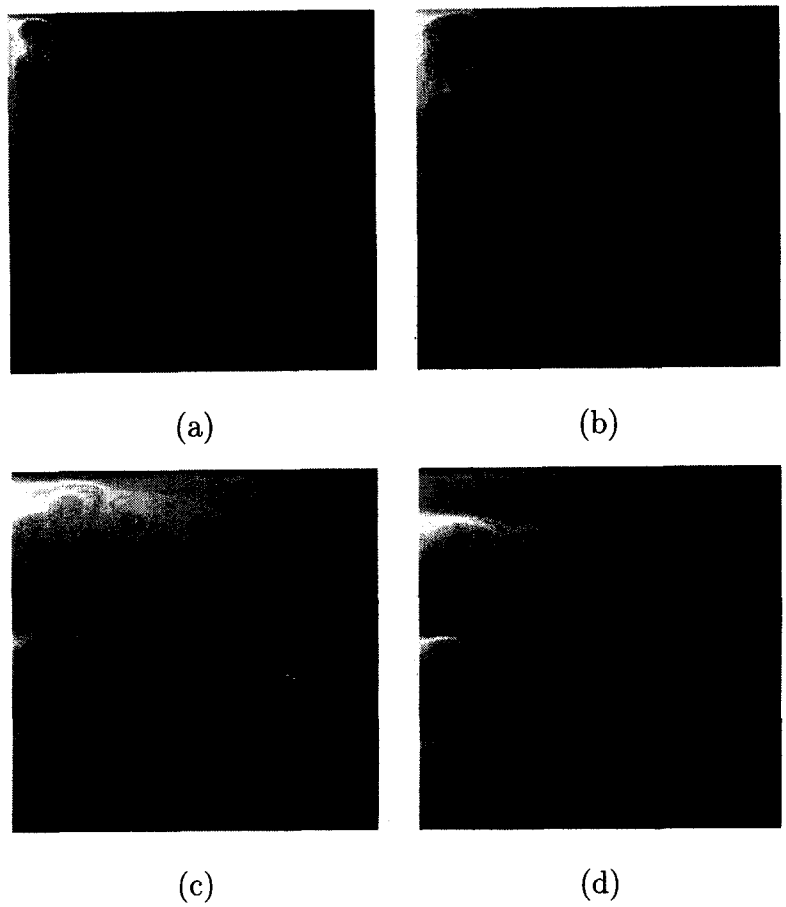

Fig. 2. Development of layers in the doubly stratified case for $Ra_\eta = 5 \times 10^4$, $R = 5$. Shown is the salinity distribution minus the initial salinity distribution. (a) $t = 0.005$; (b) $t = 0.01$; (c) $t = 0.05$; (d) $t = 0.1$.

attributed to salt-fingering, with localized areas where direct buoyancy induced convection occurs. As the forcing is turned off, the stabilizing influence of the temperature distribution decreases since thermal diffusion is fast (Fig. 6(d)). The salt transport to the top of the upper layer decreases and consequently maxima in salinity appear within the upper layer (clearest seen in Fig. 6(e) at $x = 1.0$). The influence on the density is such that the distribution remains stably stratified (Fig. 6(f)). At $t = 0.09$, the temperature profiles have reversed near the top of the upper layer (Fig. 6(g)) and a maximum in the temperature appears near $z = 0.8$ at $x = 0.5$ and appears at $z = 0.7$ at $x = 1.5$. A similar shift in the maxima of the salinity profile in the upper layer is observed (Fig. 6(h)) with a larger salinity at $x = 0.5$ than at $x = 1.5$. Consequently, the isopycnals slope towards the horizontal, as can be seen in Fig. 6(i). This slope is clearly visible in a grey-shade plot of the density at the corresponding times ($t = 0.07$ and $t = 0.09$) shown in Fig. 7(a) and (b), respectively. At a later time ($t = 0.15$), this slope decreases due to adjustment (Fig. 7(c)). This corresponding density plots for the singly stratified case (Fig. 7(d)–(f)) show a much smaller slope and hardly any change with time after the forcing has been turned off.

The horizontal velocity at $x = 0.5$ (Fig. 8(a)) and $x = 1.5$ (Fig. 8(b)) for two different times during the evolution of the flow in Fig. 5(b) are shown in Fig. 8. In Fig. 8(a), the magnitude of the horizontal velocity at about $z = 0.8$ increases in time, although the forcing is off. The same is seen in Fig. 8(b), but the maximum occurs at smaller values of z ($z = 0.7$). The increase in velocity is also observed in the development of the average kinetic energy $\langle E_k \rangle$ for the flow which is plotted in Fig. 9(a). In the unforced doubly stratified flow in Fig. 5(b), $\langle E_k \rangle$ initially increases up to $t = 0.08$ and then decreases. For comparison, the evolution of $\langle E_k \rangle$ is also shown (Fig. 9(b)) for the singly stratified flow in Fig. 5(c). As is expected, $\langle E_k \rangle$ decreases immediately as the forcing is turned off due to viscous dissipation.

The flow shown in Fig. 5(b) and its characteristics presented above are a clear example of self-propagation. The main question is how to describe the physics of this phenomenon and identify its energy sources. Reference [6] suggests that local instabilities induced by liquid blocking due to endwall effects [1] are the

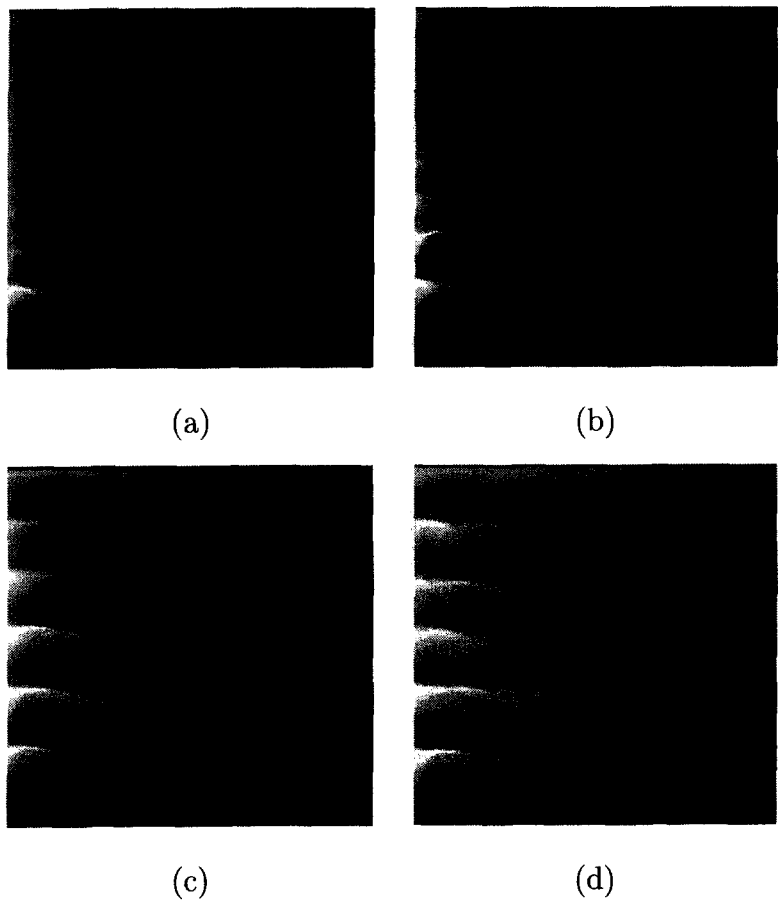

Fig. 3. As Fig. 2, but now for the singly stratified case at the same instants.

main energy source of self-propagation. Characteristic of liquid blocking is a weak upward and downward flow just ahead of the intrusion. This flow disturbs the stabilizing salinity distribution but leaves the unstable temperature distribution merely intact due to the much larger thermal diffusivity. Hence, the value of R_ρ is locally reduced and local instabilities provide the energy for the intrusion to grow.

To test this hypothesis, the flow just ahead of the intrusions is considered during the self-propagation stage. The stream function field (Fig. 10(a)), a vector plot of the velocity (Fig. 10(b)) and the R_ρ field (Fig. 10(c)) are shown just ahead of the propagating intrusion [detail of Fig 5(b)(iv)]. Note the different vertical scale in this plot, compared to the ones in Fig. 5(b). Although there is a weak buoyancy driven flow ahead of the intrusions, there are no signatures of a blocked flow ahead of the intrusion (Fig. 10(a)–(b)). The background flow is nearly parallel and returns only in a thin boundary layer near the right wall. The black regions in Fig. 10(b) indicate values of $R_\rho < 1$ and show that the flow ahead of the intrusion is statically unstable. This is caused by an unstable thermal stratification and a strongly reduced salinity gradient. Figure 11(a)–(c) show that the temperature field farther ahead of an intrusion is indeed undisturbed, but that the salinity field is affected by the weak background flow. The vertical scale over which the unstable stratification occurs is sufficiently large (about 0.1 units) to cause a buoyancy driven direct instability. Even if the stratification is stable, double-diffusive instabilities may cause growth of perturbations ahead of the intrusions.

However, the origin of the weak background flow is the gravitational adjustment associated with the sloping isopycnals and is not related to any blocking. This can be seen in the Fig. 5(b) (panels (iii) and (iv)), where the flow in the upper layer is to the right along the first interface, just as one would expect from an adjustment. Moreover, one can observe the adjustment in Fig. 7(a)–(c). Hence, local instabilities may provide an energy source of the self-propagation of the intrusions, but only in the presence of such a weak background flow, induced by adjustment.

4. CONCLUSIONS

The results from the two-dimensional numerical simulations of the evolution of intrusions into a stratified liquid show many features also observed in exper-

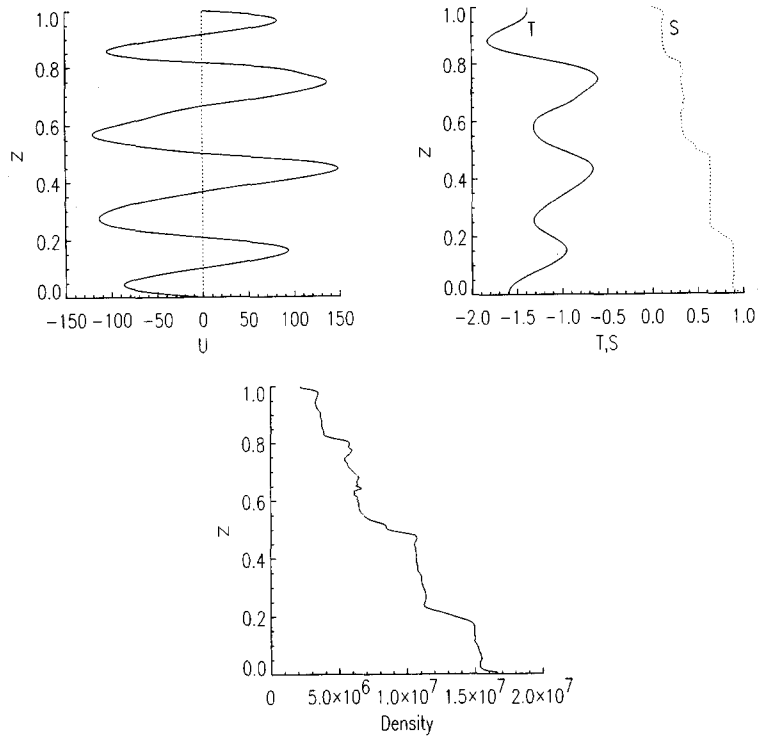

Fig. 4. Horizontal velocity U, temperature T, salinity S and density ρ for the doubly stratified case at $t = 0.1$ along a section through the middle of the container.

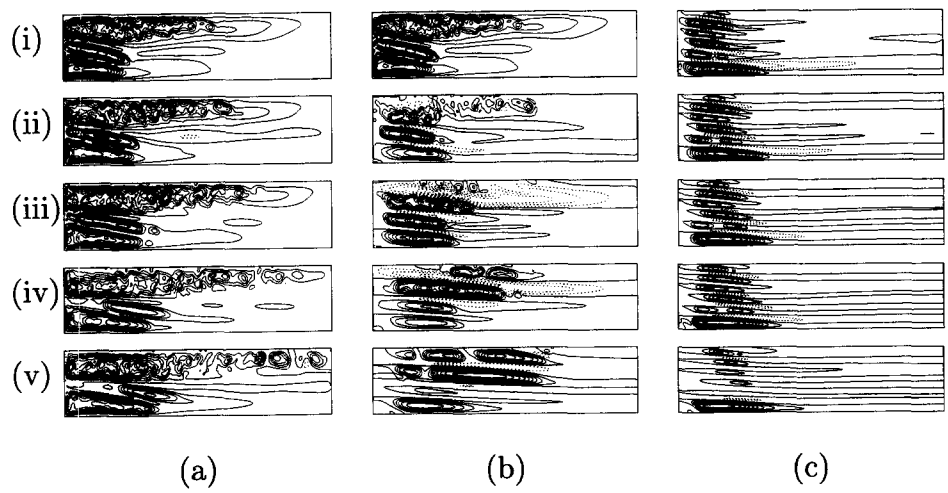

Fig. 5. Flow development from $t = 0.05$ for both doubly stratified and singly stratified cases, for $A = 4$. (a) doubly stratified, thermal forcing continued; (b) doubly stratified, no thermal forcing; (c) singly stratified, no thermal forcing. Time intervals: (i) $t = 0.05$; (ii) $t = 0.06$; (iii) $t = 0.07$; (iv) $t = 0.09$; (v) $t = 0.1$.

iments. This *a posteriori* justifies the use of the two-dimensional model; the dominant physics of layer formation and self-propagation is already captured by such a model.

The analysis of the flow details lead to the following physical picture of self-propagation in doubly stratified systems. If R_ρ is small enough, the upward transport of salt along the heated wall is able to cause intense convection in the upper layer through salt-fingering (or direct instabilities). This cannot be accomplished in a single stratified liquid, because (i) the initial temperature distribution does not destabilize the flow and (ii) the layer thickness does not increase but decreases upwards. Hence, most of the salt is

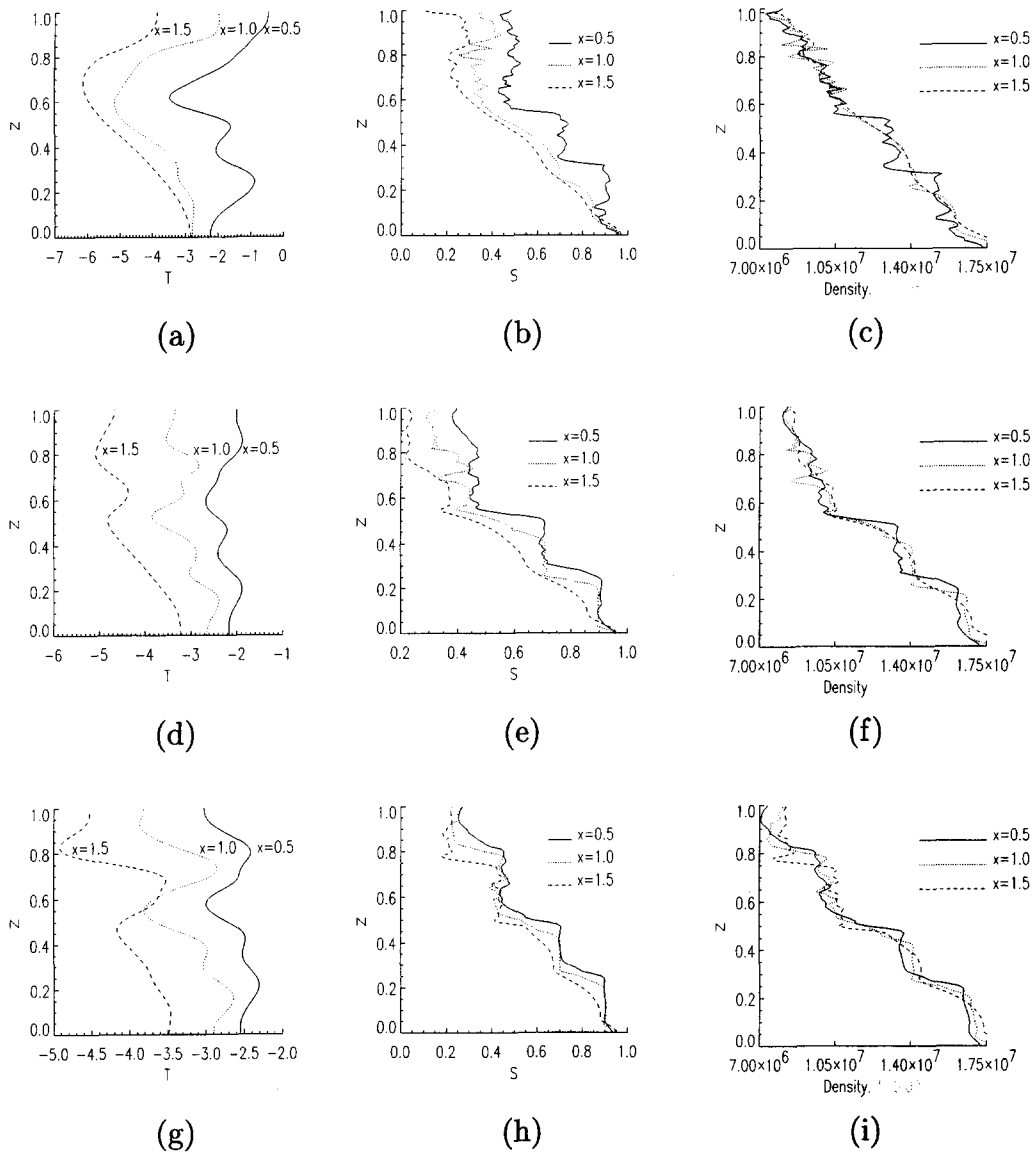

Fig. 6. Vertical sections of temperature, salinity and density for the doubly stratified ($A = 4$) case at several instants; (a–c) $t = 0.05$; (d–f) $t = 0.07$; (g–i) $t = 0.09$.

transported by the lowest layers in this case, contrary to that in the doubly stratified case, where most salt is transported by the most upper layer.

As the forcing is turned off, a horizontal salt gradient results because near the heated wall more salt has accumulated than far from that wall. Contrary to the temperature distribution, the salinity distribution recovers slowly. Consequently, a relatively strong slope in the isopycnals results when the sidewall heating is turned off. During the unforced evolution, the liquid adjusts itself and the heavier liquid moves to its neutral level. This sets up a background flow and provides a simple source of energy of self-propagation. Due to the presence of the background flow the salinity field is modified just ahead of the intrusion whereas the temperature field is hardly modified because of relatively large thermal diffusion. Local instabilities, which may be direct or double diffusively driven, may provide kinetic energy to the intrusion.

Hence, the heart of the physics of the self-propagation is the slope of the isopycnals set-up by the differential salt transport in the upper layer due to salt fingering. This slope provides itself an energy source due to adjustment and provides the background flow such that local instabilities may occur. When the stability ratio increases, both sources of energy are much weaker since the slope in the isopycnals is much smaller and no background flow (and consequently no local instabilities) occurs. This description therefore explains why self-propagation does not occur in a singly stratified system.

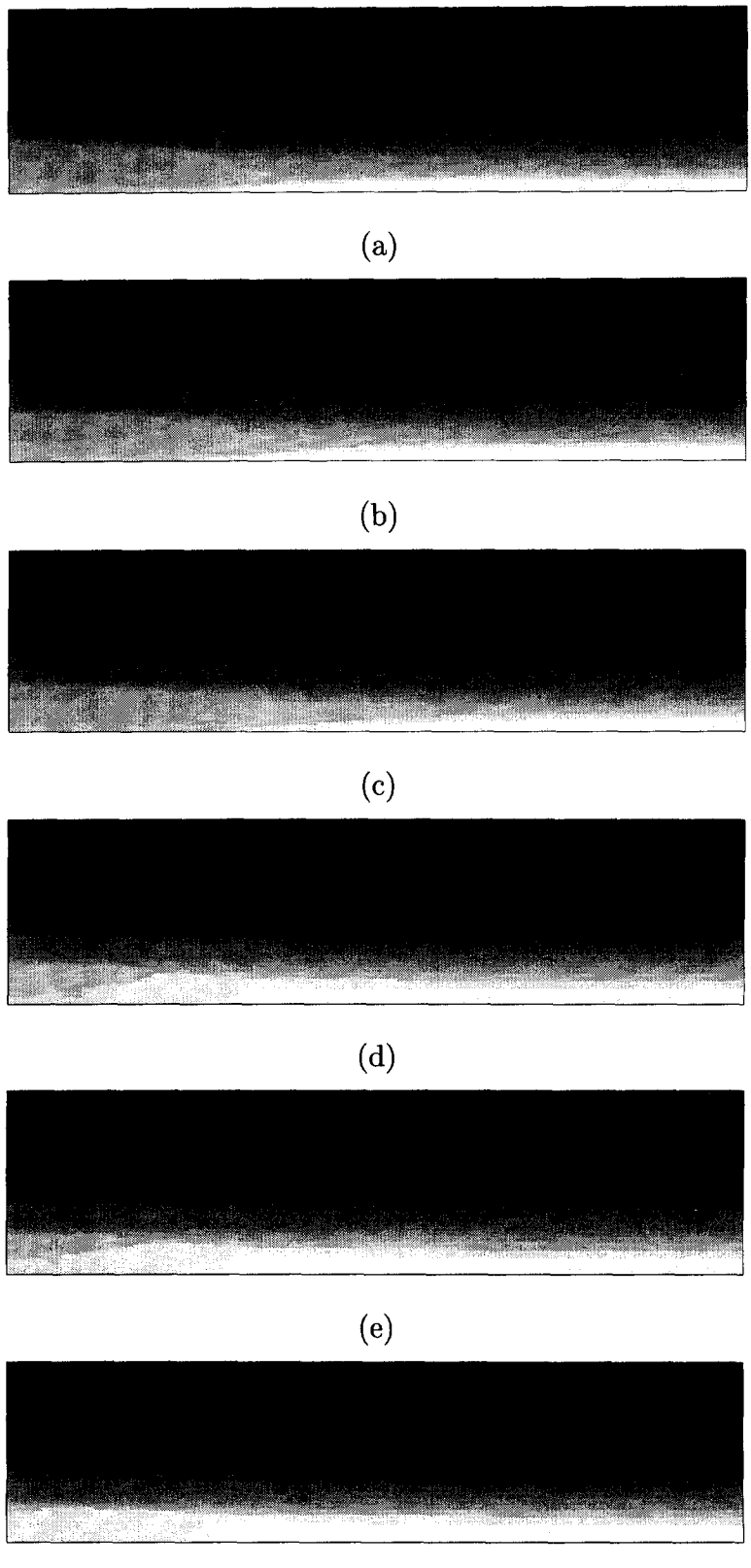

Fig. 7. Density grey-shade plots for the doubly stratified case (a–c) and the singly stratified case (d–f) when the thermal forcing has been shut-off. (a, d) : $t = 0.07$ (panel (iii) in Fig. 5), (b, e) : $t = 0.09$ (panel (iv) in Fig. 5), (c, f) : $t = 0.15$ (panel (v) in Fig. 5).

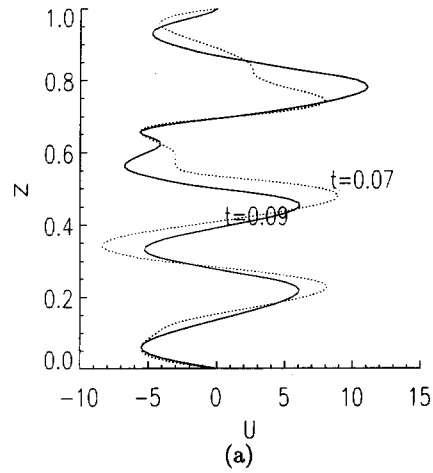

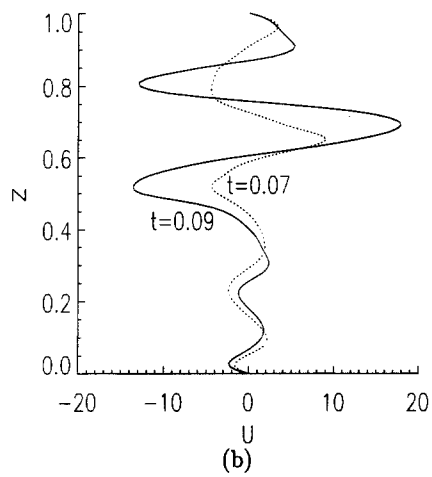

Fig. 8. Vertical section of the horizontal velocity at $x = 0.5$ (a) and $x = 1.5$ (b) for two different times.

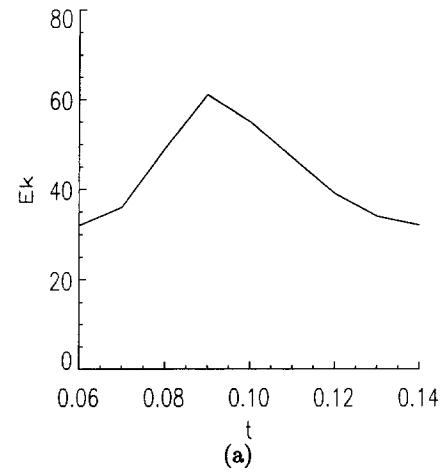

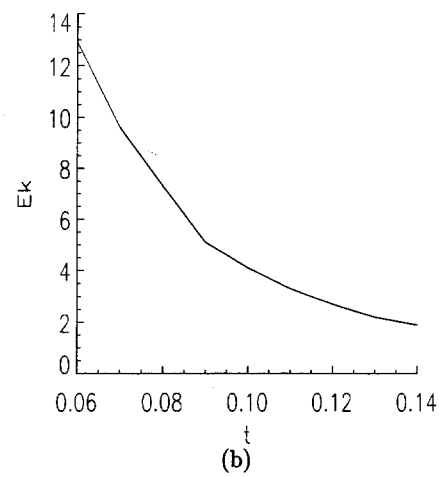

Fig. 9. Change in $\langle E_k \rangle$ with time when thermal forcing has been shut-off; (a): doubly stratified case (Fig. 5(b)), (b): singly stratified case (Fig. 5(c)).

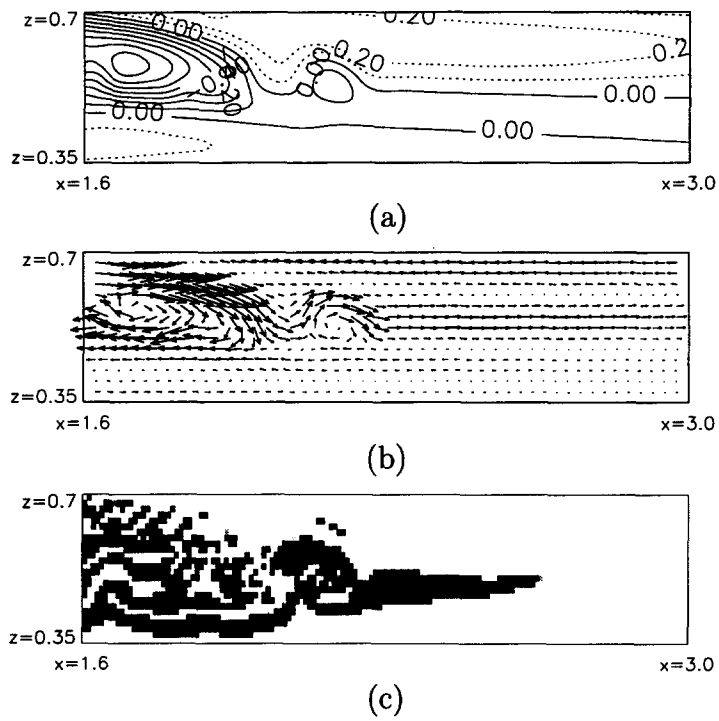

Fig. 10. Detail of the intrusion front in Fig. 5(b) (panel (iv)) for the doubly stratified case; (a): ψ near intrusion front, (b) velocities (for clarity a reduced number of vectors is shown), (c) R_ρ, black regions correspond to $R_\rho < 1$.

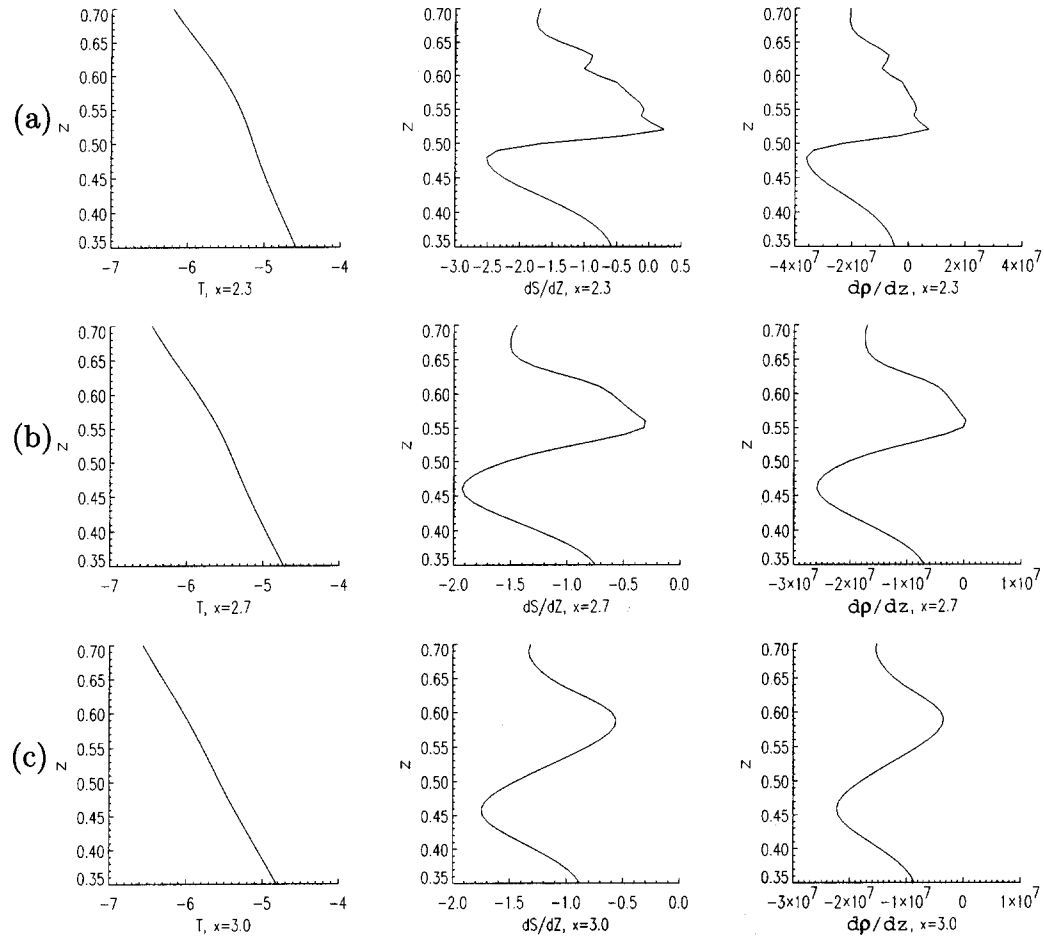

Fig. 11. Vertical sections of temperature, vertical salinity gradient and vertical density gradient ahead of the intrusion front; (a) $x = 2.3$, (b) $x = 2.7$, (c) $x = 3.0$.

Acknowledgements—All computations were performed on the CRAY C98 at the Academic Computing Centre (SARA), Amsterdam, The Netherlands within the project SC212. Use of these computing facilities was sponsored by the Stichting Nationale Supercomputer Faciliteiten (National Computing Facilities Foundation, NCF) with financial support from the Nederlandse Organisatie voor Wetenschappelijk Onderzoek (Netherlands Organization for Scientific Research, NWO). The authors thank Jeroen Molemaker for the use of the explicit CFD code and for comments on the results.

REFERENCES

1. Turner, J. S., *Buoyancy Effects in Fluids*. Cambridge, 1973.
2. Schmitt, R. W., Double diffusion in oceanography. *Ann. Rev. Fluid Mech.*, 1994, **26,** 255–285.
3. Wirtz, R. A., Briggs, D. G. and Chen, C. F., Physical and numerical experiments on layered convection in a density–stratified fluid. *Geophysical and Astrophysical Fluid Dynamics*, 1972, **3,** 265–288.
4. Jeevaraj, C. and Imberger, J., Experimental study of double-diffusive instability in sidewall heating. *Journal of Fluid Mechanics*, 1991, **222,** 565–586.
5. Kranenborg, E. J. and Dijkstra, H. A., On the evolution of double-diffusive intrusions into a stably stratified liquid : a study of the layer merging process. *International Journal of Heat and Mass Transfer*, 1998 (in press).
6. Schladow, S. G., Thomas, E. and Koseff, J. R., The dynamics of intrusions into a thermohaline stratification. *Journal of Fluid Mechanics*, 1992, **236,** 127–165.
7. Jacobs, S. S., Huppert, H. E., Holdsworth, G. and Drewry, D. J., Thermohaline steps induced by melting of the Erebus Glacier tongue. *J. Geophys. Res.*, 1981, **86,** 6547–6555.